Applied Catalysis B: Environmental 123–124 (2012) 257–264

Contents lists available at SciVerse ScienceDirect

Applied Catalysis B: Environmental

journal homepage: www.elsevier.com/locate/apcatb

Copper and iodine co-modified TiO_2 nanoparticles for improved activity of CO_2 photoreduction with water vapor

Qianyi Zhang[a], Tingting Gao[b], Jean M. Andino[b,c], Ying Li[a,*]

[a] University of Wisconsin-Milwaukee, Department of Mechanical Engineering, Milwaukee, WI 53211, USA
[b] Arizona State University, Civil, Environmental, and Sustainable Engineering, Tempe, AZ 85287, USA
[c] Arizona State University, Chemical Engineering, Tempe, AZ 85287, USA

ARTICLE INFO

Article history:
Received 16 January 2012
Received in revised form 10 April 2012
Accepted 23 April 2012
Available online 28 April 2012

Keywords:
Photocatalysis
CO_2 reduction
Solar energy
TiO_2
Copper
Iodine

ABSTRACT

Copper and iodine co-modified TiO_2 nanoparticles (Cu–I–TiO_2) were synthesized through a combined hydrothermal and wet-impregnation process. The structures and properties of the catalysts were characterized by XRD, BET, SEM/EDX, XPS, and UV–vis diffuse reflectance spectroscopy. Iodine ions were doped in the TiO_2 lattice by replacing Ti^{4+} and, consequently, Ti^{3+} was generated to balance the charge. Iodine doping reduced the TiO_2 crystal size and was responsible for visible light absorption. Cu species were found to deposit on the surface of TiO_2 and resulted in a slightly increased particle size. The activity of the Cu–I–TiO_2 catalyst was investigated by the photocatalytic reduction of CO_2 with water vapor, and CO was found to be the major reduction product with trace amounts of CH_4 generated. Under UV–vis irradiation, the activity of the co-modified catalyst (Cu–I–TiO_2) was higher than that of the single ion-modified catalysts (Cu–TiO_2 or I–TiO_2). Under visible light irradiation, the addition of Cu to I–TiO_2 did not lead to significant improvements in CO_2 reduction. Methyl chloride (CH_3Cl) was detected as a reaction product when $CuCl_2$ was used as the precursor in the synthesis, thus suggesting that methyl radicals are reaction intermediates. When $CuCl_2$ was used as the Cu precursor, a three-fold increase in CO_2 photoreduction activity was observed, as compared to when $Cu(NO_3)_2$ was used as the Cu precursor. These differences in activities were probably due to enhanced Cu dispersion and the hole-scavenging effects of the Cl ions. However, the formation of by-products (e.g., CH_3Cl) may be undesirable.

1. Introduction

There have been increased concerns about global climate change as well as worldwide interest in reducing the emissions of greenhouse gases (GHG), particularly carbon dioxide (CO_2) [1]. Conversion of CO_2 to valuable energy-bearing compounds (such as CO, methane, and methanol) offers a brand new opportunity for a sustainable energy future. Photocatalytic reduction of CO_2 has been studied since 1979 when Honda and co-workers first demonstrated the conversion of CO_2 to organic compounds in an aqueous suspension of oxide and non-oxide semiconductor particles under ultraviolet (UV) irradiation [2]. Among the various photocatalysts that have been studied for CO_2 photoreduction, TiO_2 is considered the most convenient candidate in terms of stability, cost, and nontoxicity [3–7]. However, the major challenge in using TiO_2 is its wide band gap (~3.2 eV for anatase and 3.0 eV for rutile). As a result, TiO_2 only responds to UV light, which accounts for less than 5% of the total solar energy. Other challenges in the area of CO_2 photoreduction are the low CO_2-to-fuel conversion rate (usually on the order of μmol per gram of catalyst per hour) due to fast electron–hole recombination, poor understanding of the reaction mechanism, and uncontrolled product selectivity [8,9].

In order to increase the photocatalytic activity of TiO_2, many studies have been conducted to modify TiO_2 with ions/species to form nanocomposites. The incorporation of noble metals or transitional metal ions in TiO_2 has been intensively investigated [10–12]. Loading metal nanoparticles onto TiO_2 leads to a redistribution of charges and formation of a Schottky barrier. Electrons migrate from the TiO_2 to the metal, and charge recombination can be suppressed [13]. The incorporation of transition metal ions (e.g., Cu^{2+}, Cu^{+}, Fe^{3+}, etc.) can also lead to the formation of electron trapping sites and promote charge transfer from TiO_2 to metal ions, thus resulting in the enhanced photoreaction of surface adsorbed species [14–16]. For example, Xu et al. [14] suggested that the Cu (identified as Cu^{+}) species that were deposited on TiO_2, forming Ti–O–Cu surface bonds, served as acceptors of electrons that were transferred from the TiO_2 conduction band. While metal modifications of TiO_2 lead to apparent enhancements in charge separation, their effects in altering the optical properties of TiO_2 are limited for most catalysts

* Corresponding author. Tel.: +1 414 229 3716; fax: +1 414 229 6958.
E-mail address: liying@uwm.edu (Y. Li).

0926-3373/$ – see front matter © 2012 Elsevier B.V. All rights reserved.
http://dx.doi.org/10.1016/j.apcatb.2012.04.035

that are prepared using wet-chemistry methods [3,16–18]. An ion implantation method results in more effective doping of metal ions in the TiO_2 lattice, and hence extends the TiO_2 absorption spectrum to the visible light range [19]. However, excess doping of metal ions into the TiO_2 lattice can result in the formation of electron–hole recombination centers [20,21].

Doping of nonmetal ions (e.g., N, S, C, F, etc.) into the TiO_2 lattice has also been widely reported to modify the nanostructure and optical properties [22–24]. These dopants create intra-band-gap states close to the conduction or valence band edges that induce visible light absorption. Unlike metal ions, nonmetal ions are less likely to form recombination centers, and thus are more effective in enhancing visible light activity [21]. Recently, the less studied iodine-doped TiO_2 has been explored, and some advantages of the iodine dopant over other nonmetal dopants have been reported [25–29]. First, substitution of a titanium atom with iodine leads to generation of Ti^{3+} that may trap photoinduced electrons and inhibit charge recombination [28]. Second, iodine atoms prefer to be doped near the TiO_2 surface due to the strong I–O repulsion, and act as surface trapping centers for electrons [27,29]. Hence, iodine doping not only leads to a red-shift in the TiO_2 light absorption spectrum, but also enhances charge separation.

Our previous research [4] for the first time tested the activity of iodine-doped TiO_2 for CO_2 photoreduction. I–TiO_2 demonstrated significant enhancements in CO_2 photoreduction to CO as compared to undoped TiO_2 under both visible light and UV–vis illumination. Interestingly, for iodine doping higher than a certain level (i.e., nominal 10 wt%), the activity of I–TiO_2 under UV–vis illumination was not superior to that seen under visible light [4]. The formation of recombination centers at high doping levels may account for this phenomenon, but further investigation is needed to better understand the mechanism. On the other hand, one of our previous studies also showed high CO_2 photoreduction activity using a Cu/TiO_2 catalyst dispersed on a mesoporous silica support [3]. Given that either metal modification or nonmetal doping can improve the photocatalytic activity of TiO_2, a new composite catalyst was fabricated in this work by incorporating both Cu and I species into TiO_2. Our hypothesis was that co-modification of TiO_2 with Cu and I would maintain the charge balance and avoid formation of recombination centers, and thus the catalyst could perform more effectively under UV–vis illumination while maintaining a high activity under visible light.

There have been literature reports that suggest that co-doping of metal and nonmetal species on TiO_2 leads to enhanced photocatalytic activity as compared with single ion-doped TiO_2 [20,30,31]. Examples include co-doping of Cu and S on TiO_2 for improved methyl orange degradation under visible light [31], Fe and N co-doped TiO_2 for narrowed band gap and enhanced photoactivity toward degradation of diphenylamine [32], and Zr and I co-doped TiO_2 for enhanced methyl orange degradation as compared to I/TiO_2 because of a smaller crystal size and higher surface area [33]. Unfortunately, most of those literature publications focused on the applications of photocatalytic oxidation of organic compounds; metal and nonmetal co-modified TiO_2 for photocatalytic CO_2 reduction has been reported only once in the literature. Varghese et al. [34] synthesized N-doped TiO_2 nanotube arrays sputtered with Pt or Cu nanoparticles as a co-catalyst and tested the catalytic activity for CO_2 reduction with water under sunlight. The product yields under visible light irradiation contributed to only 3% of that under the entire solar spectrum, implying a limited rate for visible light utilization [34]. The raw materials used in the work of Varghese et al. [34] were expensive and the fabrication process was relatively complicated. In this work, we used a much simpler method and cheaper raw materials to synthesize Cu and I co-modified TiO_2 nanoparticles. The catalytic activities for the photocatalytic reduction of CO_2 with water vapor under visible and UV–visible illumination are compared, and new insights regarding the reaction mechanism are proposed in this paper.

2. Experimental

2.1. Synthesis of Cu–I modified TiO_2 catalysts

Copper chloride dyhydrate ($CuCl_2{\cdot}2H_2O$, >99%, Acros Organics), iodic acid (HIO_3, >99.5%, Alfa Aesar), and titanium isopropoxide (TTIP, >99.5%, Acros Organics) were used as the precursors for Cu, I, and TiO_2, respectively. A two-step process modified from the literature [3,4,27] was used to prepare Cu and I co-modified TiO_2 (Cu–I–TiO_2). The first step was to synthesize I-doped TiO_2 through a hydrothermal method reported in our previous study [4]. Briefly, a mixture of TTIP and isopropanol was first added dropwise into a HIO_3 solution under continuous stirring for 2 h, and the resultant mixture was transferred to a Teflon-lined vessel for hydrothermal treatment at 100 °C for 12 h. After that, the particles were filtered and washed with copious amounts of de-ionized water until pH 7. Finally, the I–TiO_2 powders were obtained by drying at 80 °C for 1 h and calcination in air for 2 h at 375 °C. The nominal iodine concentration and calcination temperature were kept at 10 wt% and 375 °C, respectively, because these parameters corresponded to an optimum activity under visible light, as reported in our previous work [4]. The second step in the synthesis process was to incorporate Cu into I–TiO_2 through an incipient wet impregnation process. Typically, 500 mg of the I–TiO_2 sample was mixed in a 20 ml $CuCl_2$ solution for 1 h, and then the mixture was dried in a vacuum oven at 80 °C for 12 h and calcined at 300 °C for 1 h. The nominal Cu concentration varied from 0.1 to 1 wt%, a range that corresponded to optimum catalytic activities reported in many studies for Cu-loaded TiO_2 [3,35,36]. The samples are denoted by "*x*Cu–*y*I–TiO_2", where *x* and *y* are the nominal weight percentages of Cu and I, respectively. For comparison, pure TiO_2, Cu–TiO_2, and I–TiO_2 were also prepared using the same procedure. In addition, to investigate the potential effect of the Cu precursor (i.e., to compare with $CuCl_2$), additional samples using different Cu precursor solutions (1) $Cu(NO_3)_2$ and (2) $Cu(NO_3)_2$ + KCl with (Cu:Cl = 1:2) were also prepared using the same procedure. All of the samples were grinded to powders and sieved by a 45 μm stainless steel sieve before the characterization and photoactivity tests.

2.2. Catalyst characterization

The crystal structure of the catalysts was characterized by X-ray diffraction (XRD) and the patterns were obtained on a Sintag XDS 2000 diffractometer using Cu Kα radiation. The acceleration voltage was 45 kV, and the emission current was 40 mA. The diffractograms were recorded in the 2θ range from 20° to 70° at a scan rate of 1°/min. The crystal size of different crystal phases were calculated using the Scherrer equation. The fractional phase contents of TiO_2 (i.e., anatase and brookite) were calculated using a previously reported method [4,37]. Brunauer–Emmett–Teller (BET) surface area analyses by N_2 adsorption were performed using a Micromeritics Tristar II 3020 instrument. Morphological information and elemental mapping of the catalyst particles were obtained by a Hitachi S570 scanning electron microscope (SEM) system equipped with energy-dispersive X-ray (EDX) spectroscopy. The UV–vis reflectance spectra were recorded with a UV–vis spectrophotometer (Ocean Optics) using $BaSO_4$ as the background. To characterize the surface atomic concentration and chemical states, X-ray photoelectron spectroscopy (XPS) measurements were performed on a VG ESCALAB 220I-XL instrument equipped with Al Kα (1486.6 eV) X-ray source.

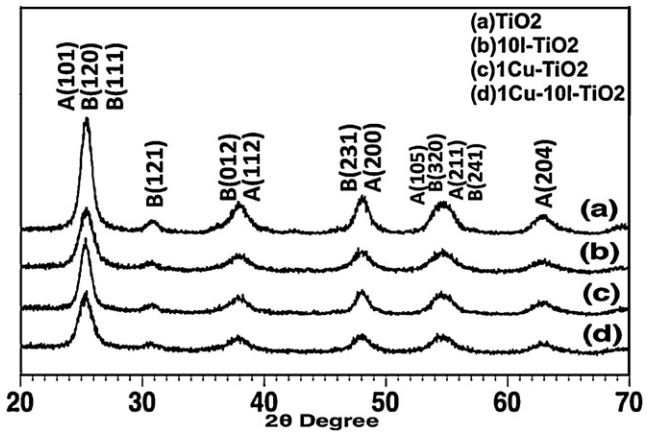

Fig. 1. XRD patterns of TiO_2 (a), 10I–TiO_2 (b), 1Cu–TiO_2 (c), and 1Cu–10I–TiO_2 (d) samples (A = anatase; B = brookite).

2.3. CO_2 photoreduction activity measurements

The experimental system used for photocatalytic CO_2 reduction was similar to that reported in our previous work [4]. Compressed CO_2 (99.999%, Praxair), regulated by a mass flow controller, was passed through a water bubbler to generate a CO_2 and H_2O vapor mixture (H_2O concentration = 2.3% by volume). The gas mixture was then purged through a cylindrical photoreactor (D = 7 cm; V = 164 cm^3) with stainless steel walls and a quartz window. A fixed amount of powder catalyst (100 mg) was dispersed onto a glass-fiber filter and placed at the bottom of the reactor. All tested catalyst samples were pre-treated under UV irradiation (12 W, 365 nm) for 12 h in air atmosphere to eliminate any possible organic residues that were left on the catalysts from the syntheses processes. After purging with a CO_2 and H_2O mixture for 1 h, the gas valves on both sides of the reactor were closed to seal the reactor so that the photocatalytic reaction was undertaken in a batch mode. A 450 W Xe lamp (Oriel) was used as the light source, and a long-pass filter was applied to cut off the short wavelengths that were less than 400 nm if only visible light was needed. A spectroradiometer (International Light Technologies ILT950) was used to obtain the spectral intensity of the Xe lamp with and without the UV filter. During the illumination period, the gaseous samples in the reactor were taken using a gastight syringe (Hamilton, 1750 series, 500 μl) every 30 min and manually injected to a gas chromatograph (GC, Agilent 7890A) equipped with both a thermal conductivity detector (TCD) and a flame ionization detector (FID). A mass spectrometer (Agilent 5795 MSD) was used together with another GC (GC/MS) to identify any unknown or unexpected species from the reaction products.

3. Results and discussion

3.1. Characteristics of Cu–I–TiO_2 catalysts

Fig. 1 shows the X-ray diffraction (XRD) patterns of pure TiO_2, 10I–TiO_2, 1Cu–TiO_2, and 1Cu–10I–TiO_2. For all samples, the characteristic peaks at $2\theta = 25.2^\circ$ and $2\theta = 30.8^\circ$ indicate the (1 0 1) plane of anatase (JCPDS 21-1272) and (1 2 1) plane of brookite (JCPDS 29-1360) TiO_2. No characteristic peak of the rutile phase ($2\theta = 27.4^\circ$) was detected. The XRD pattern did not show any copper or iodine phase. Calculated values of the crystal phase contents and crystal sizes appear in Table 1. The pure TiO_2 consisted of 70% anatase and 30% brookite, with a crystal size of 8.9 nm for anatase and 4.8 nm for brookite. The BET surface area of TiO_2 was relatively high (117.3 m^2/g) as compared to commercial P25 TiO_2 (~50 m^2/g), likely due to its smaller primary particle size (less than 10 nm) as compared to that of P25 (~20 nm). The incorporation of iodine doping (10I–TiO_2) did not appear to change the phase content, but significantly reduced the crystal size of anatase to 5.6 nm. The smaller crystal size due to lattice doping that was detected in this work agrees with those reported in the literature [4,26,38]. Accordingly, the surface area of 10I–TiO_2 (128.2 m^2/g) was higher than that of pure TiO_2. The incorporation of Cu (i.e., 1Cu–TiO_2) slightly reduced the anatase content and increased the anatase crystal size, and, consequently, its surface area decreased to 95.3 m^2/g. This trend agrees with the result reported by Slamet et al. [39] that Cu-loaded TiO_2 had a smaller surface area as compared to bare TiO_2. This also implies that through the wet impregnation process, Cu species are deposited on the surface of TiO_2 rather than in the lattice. The combination of both Cu and I modification (i.e., 1Cu–10I–TiO_2) resulted in a sample with the expected characteristics, i.e., similar phase content as 1Cu–TiO_2 (since iodine does not affect the phase content) and an anatase crystal size that was in between that of 1Cu–TiO_2 and 10I–TiO_2 (Cu increased while I reduced the TiO_2 crystal size). Interestingly, the surface area of 1Cu–10I–TiO_2 was the highest (146.4 m^2/g) among all the measured samples, which may relate to its smallest brookite crystal size, as shown in Table 1. Unlike anatase, the crystal size of brookite does not apparently relate to the catalyst composition. Brookite TiO_2 is much less studied in the literature and the lack of understanding of doped brookite warrants further investigation.

Table 1
Phase content and average size of Cu–I–TiO_2 samples obtained from X-ray diffraction, bad gap from optical spectroscopy, and specific surface area from BET analysis (A: anatase; B: brookite).

	Phase content (%)		Crystal size (nm)		BET (m^2/g)
	A	B	A	B	
TiO_2	70	30	8.9	4.8	117.3
10I–TiO_2	67	33	5.6	5.3	128.2
1Cu–TiO_2	54	46	9.6	4.1	95.3
1Cu–10I–TiO_2	58	42	6.9	3.7	146.4

Fig. 2 shows the results of SEM/EDX analyses of the 1Cu–10I–TiO_2 sample. Agglomerates of TiO_2 nanoparticles were observed in the SEM image. No textural difference was found in the SEM images between pure TiO_2, single ion-modified, and co-modified TiO_2 samples. The EDX analyses confirm the presence of Cu and I in the TiO_2 sample. In addition, the element of Cl was also identified (at 2.6 keV), since $CuCl_2$ was used as the Cu precursor in the wet-impregnation process.

The UV–vis diffuse reflectance spectra (converted to absorbance) of pure TiO_2, 1Cu–TiO_2, 10I–TiO_2 and Cu–10I–TiO_2 samples with different Cu concentrations are shown in Fig. 3. The

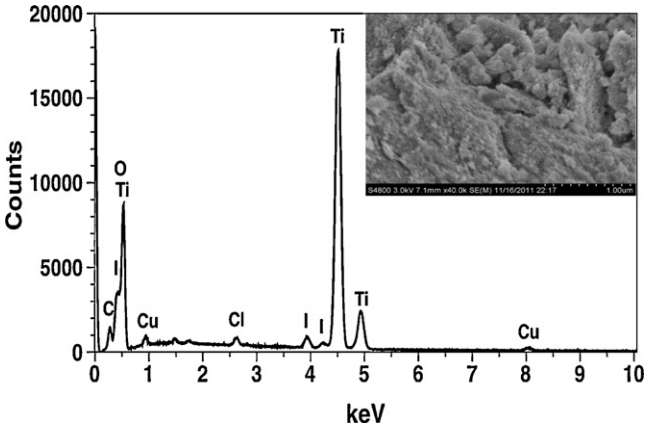

Fig. 2. EDX analysis and SEM image (inset) of 1Cu–10I–TiO_2 sample.

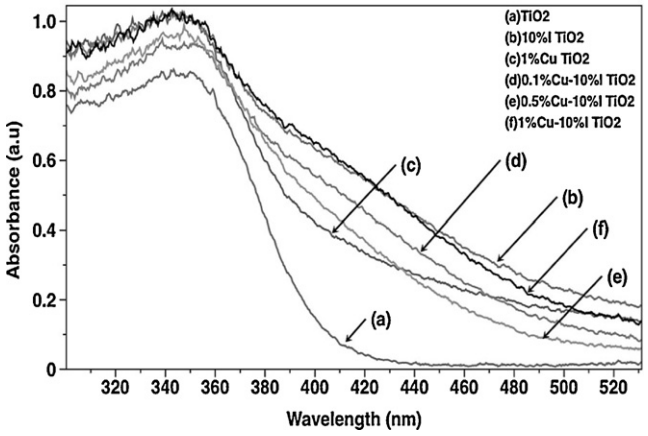

Fig. 3. UV–vis diffuse reflectance spectra of the catalyst samples displayed in absorbance.

absorption edge of pure TiO_2 is around 400 nm. For the 1Cu–TiO_2 sample, the absorption edge is only slightly shifted as compared to pure TiO_2. This result is in agreement with our previous research that suggested that impregnation of Cu on TiO_2 did not have a prominent effect on the optical property [3]. For all I-doped TiO_2, with or without Cu, the absorption edge shifted to the visible region, in agreement with the yellow color of the I-doped TiO_2 samples. The Cu concentration on the Cu–10I–TiO_2 samples (at a constant I doping level) did not significantly affect the light absorption. These optical properties support the conclusions that Cu that is deposited on the surface does not change the TiO_2 band structures, and iodine that is doped in the lattice may generate intra-band-gap states in TiO_2.

The chemical states of the component elements of the catalyst were analyzed by XPS. The XPS survey spectrum for 1Cu–10I–TiO_2 is shown in Fig. 4a, and the high resolution XPS spectra of the binding energies for Ti 2p, I 3d, and Cu 2p are presented in Fig. 4b–d. The survey spectrum indicates the presence of Ti, O, I and Cu. Table 2 summarizes the surface atomic concentrations of Ti, I, O, and Cu, as well as the atomic percentages of the Ti and I elements at different chemical states. As shown in Fig. 4b, XPS features in the region of Ti 2p appear at 465.2 eV (Ti $2p_{1/2}$) and 459.7 eV (Ti $2p_{3/2}$), both of which are attributed to Ti^{4+}. The two smaller peaks at 463.4 eV (Ti $2p_{1/2}$) and 457.7 eV (Ti $2p_{3/2}$) signify the existence of Ti^{3+}. For pure TiO_2 and 1Cu–TiO_2 samples, only Ti^{4+} was detected (see Table 2 and Fig. 5e), suggesting that Ti^{3+} is generated to maintain electroneutrality due to the substitution of Ti^{4+} with I^{5+} [4,28]. As shown in Fig. 4c, the XPS spectrum of the I 3d region shows two double peaks. The two peaks around 635.2 eV (I $3d_{3/2}$) and 623.5 eV (I $3d_{5/2}$) are attributed to I^{5+}, while the other two weaker peaks around 631.9 eV (I $3d_{3/2}$) and 620.3 eV (I $3d_{5/2}$) indicate the existence of I^- [4,27,30]. The I^{5+}/I^- pairs also appear on the 10I–TiO_2 sample, but the atomic ratio of I^{5+}/I^- is likely affected by Cu (see Table 2). Comparing with the 10I–TiO_2 sample, the 1Cu–10I–TiO_2 sample has a higher I^{5+} concentration and a slightly higher Ti^{3+} concentration. This result implies that the incorporated Cu species may promote the substitution of I^{5+} in the place of Ti^{4+} in the TiO_2 lattice.

The XPS spectrum of Cu 2p is shown in Fig. 4d. The binding energy of the Cu 2p3/2 peak is 932.6 eV, and the binding energy of Cu 2p1/2 is 952.3 eV. These binding energies of the Cu 2p peaks are characteristic of Cu_2O. The binding energies of the CuO peaks are normally shifted by 1.3 eV above the Cu_2O peak, and also have shake-up satellite peaks at approximately 942 eV. The lack of shake-up satellite peaks at approximately 942 eV in Fig. 4d also suggests that Cu_2O is the primary Cu species in the 1Cu–10I–TiO_2 sample. This result agrees with many other literature reports that indicate that the dominant Cu specie is Cu(I) on Cu-loaded TiO_2 samples [3,30,40].

3.2. Catalytic activity for CO_2 photoreduction to CO

A series of background tests were first conducted to prove that any carbon-containing compounds in the effluent gas measured by the GC indeed originated from CO_2 through photocatalytic reactions. First, tests were conducted using CO_2 and H_2O vapor as the purging and reaction gases for the cases of (1) empty reactor and (2) blank glass-fiber filter in the reactor. No carbon-containing compounds were produced under either UV or visible irradiation in each of the two cases. This demonstrates that the reactor and the glass-fiber filter were clean and that the CO_2 conversion could not proceed without the photocatalyst. Second, pure helium (instead of CO_2) and water vapor were used as the purging and reaction gases, and the system was tested with the catalyst loaded in the reactor. Again, no carbon-containing compounds were produced by the catalyst under either UV or visible irradiation. This verified that the catalyst was clean (i.e., no interference from organic residues) and that any C-containing gases that were produced were derived from CO_2 in the reaction gases.

CO_2 photoreduction with water vapor over TiO_2-based catalysts was studied in a batch mode for a period of 210 min for each test. Fig. 5 shows the yield of CO from CO_2 reduction as a function of illumination time for the various catalysts under visible light ($\lambda > 400$ nm) and UV–vis irradiation ($\lambda > 250$ nm). Each sample was tested twice and the average yields and error bars are shown in Fig. 5. Under visible light, no activity of CO_2 reduction was observed for either pure TiO_2 or 1Cu–TiO_2. Thus, zero activities are not shown in Fig. 5a. This result is consistent with the inability of TiO_2 or 1Cu–TiO_2 to absorb visible light, as shown in Fig. 3. All I-doped TiO_2 samples exhibited visible light activities for CO_2 photoreduction to CO, and the production was almost linear with illumination time (Fig. 5a). Among the three Cu–10I–TiO_2 samples with different Cu concentrations (0.1, 0.5, and 1%), 1%Cu appeared to be the optimum material, having a CO production of 6.7 $\mu mol\, g^{-1}$ at 210 min. However, only the 1Cu–10I–TiO_2 sample demonstrated a higher activity than the 10I–TiO_2 sample (5.3 $\mu mol\, g^{-1}$ at 210 min) while the other two co-modified samples 0.1Cu–10I–TiO_2 and 0.5Cu–10I–TiO_2 were inferior to 10I–TiO_2. Very few studies have reported CO_2 photoreduction with water under visible light. Varghese et al. [34] used an N-doped TiO_2 nanotube array sputtered with Cu for CO_2 photoreduction with water vapor under sunlight and reported a production rate of 0.3 $\mu mol\, g^{-1}\, h^{-1}$ ascribed to the visible light portion (or 3% of the total photocatalytic activity under sunlight). Our production rate under visible light (e.g., 1.9 $\mu mol\, g^{-1}\, h^{-1}$ for 1Cu–10I–TiO_2) is much higher than that reported by Varghese et al. [34], while our raw materials are cheaper and our synthesis method is simpler, although the intensity of visible light in our work was approximately four times as much as that of sunlight.

Under UV–vis irradiation (Fig. 5b), very different activity results were observed from those under visible light. Pure TiO_2 had the lowest activity, while single ion-modified TiO_2 samples (1Cu–TiO_2 and 10I–TiO_2) exhibited enhanced, yet small activities. Cu and I co-modified TiO_2 samples had remarkably higher activities, while the 0.1%Cu sample appeared to be the best among the three Cu–10I–TiO_2 samples. While the deposited Cu species may act as hole scavengers and thus enhance the CO_2 reduction rate, the anion species (e.g., Cl^-) present on the catalyst and the dispersion of Cu species were found to have significant effects on the reaction rate and product selectivity, as discussed in Section 3.3.

Another significant result shown in Fig. 5 is that the 1Cu–10I–TiO_2 sample led to a higher level of CO production under visible light (6.7 $\mu mol\, g^{-1}$ CO production) as compared

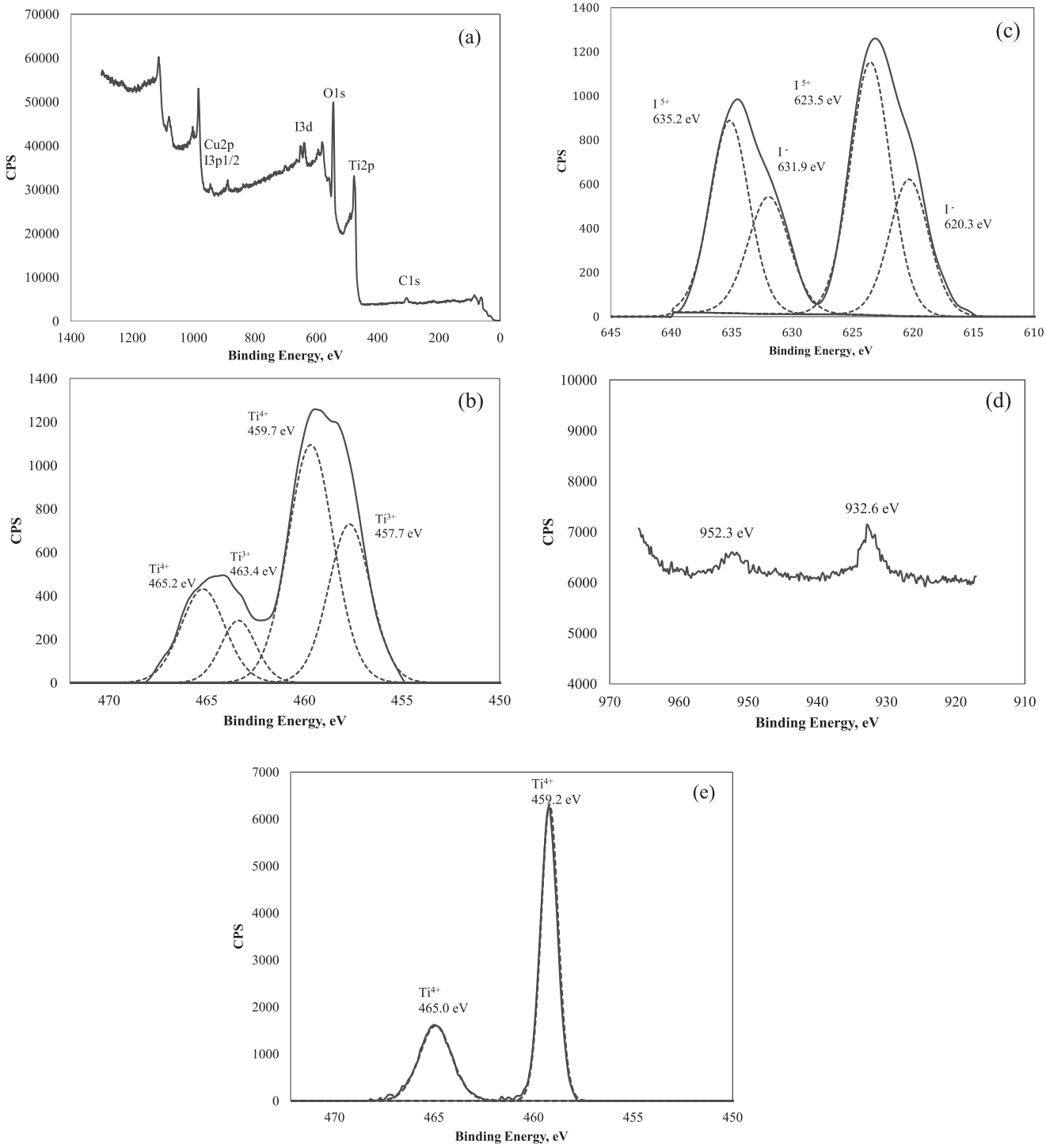

Fig. 4. XPS survey spectrum of 1Cu–10I–TiO_2 (a), high resolution XPS spectra of Ti 2p (b), I 3d (c), and Cu 2p (d) of 1Cu–10I–TiO_2, and high resolution XPS spectra of Ti 2p of pristine TiO_2 (e).

Table 2
Surface atomic concentrations of catalysts from XPS analyses.

Sample	Surface atomic concentration (%)				Ti species (%)		I species (%)	
	Ti	O	I	Cu	Ti^{4+}	Ti^{3+}	I^{5+}	I^{-}
TiO_2	27.3	72.7	n/a	n/a	100	0	n/a	n/a
10I–TiO_2	31.9	64.0	4.1	n/a	69.3	30.7	48.7	51.3
1Cu–TiO_2	28.2	71.4	n/a	0.4	100	0	n/a	n/a
1Cu–10I–TiO_2	40.0	52.0	7.7	0.3	62.8	37.2	63.2	36.8

n/a: not applicable.

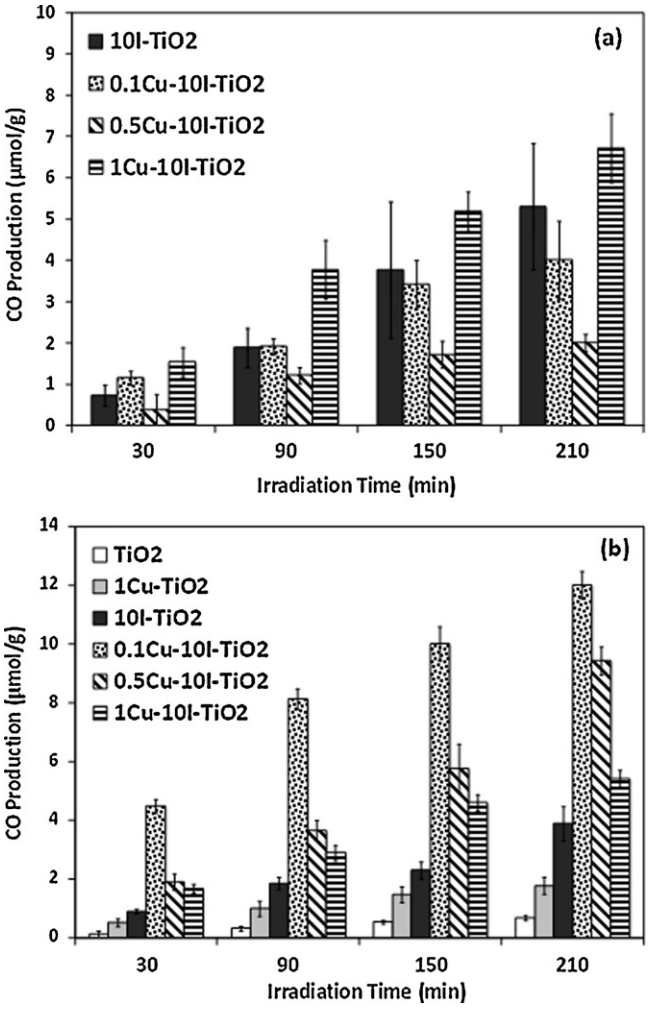

Fig. 5. CO yield under visible light irradiation (a) and UV/vis irradiation (b).

to that under UV–vis irradiation (5.4 μmol g^{-1} CO production), while the opposite trend was observed for the 0.5Cu–10I–TiO_2 and 0.1Cu–10I–TiO_2 samples. Similarly, in our previous research [4], the 10I–TiO_2 sample had a higher activity for CO_2 photoreduction to CO under visible light than under UV–vis light irradiation, while the sample with lower iodine concentration, 5I–TiO_2, had an opposite trend. In addition, in this work all three Cu–I–TiO_2 samples exhibited higher activities than the I–TiO_2 sample under UV–vis light but two out of three Cu–I–TiO_2 samples with lower Cu concentrations had lower activities than the I–TiO_2 sample under visible light. All these results suggest that the presence and concentrations of the modifiers (Cu and I) have an important role in catalytic activity with different excitation sources. A general observation is that to achieve an optimum activity, a higher modifier concentration is needed under visible light (e.g., 10I–TiO_2 rather than 5I–TiO_2 [4]; 1Cu–10I–TiO_2 rather than 0.5Cu–10I–TiO_2 and 0.1Cu–10I–TiO_2) but a lower modifier concentration is needed under UV–vis light. A possible reason is that very high modifier concentrations may lead to the formation of recombination centers, particularly when there is a larger population of photo-induced electron–hole pairs (i.e., under UV–vis light).

3.3. Product selectivity and reaction mechanism

Besides the formation of CO as a major product, two minor products, methyl chloride or chloromethane (CH_3Cl) and methane (CH_4) were also observed using certain catalysts under certain excitation

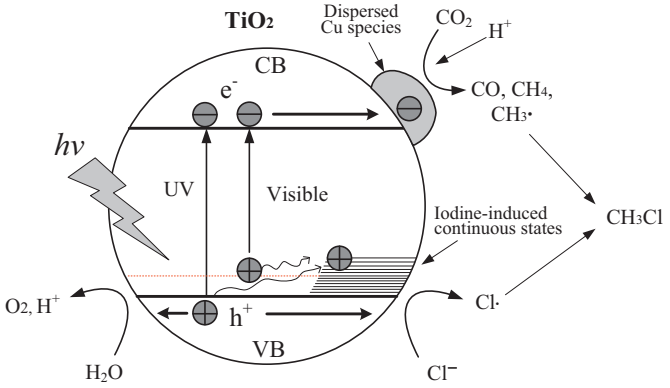

Fig. 6. Proposed reaction mechanism of CO_2 photoreduction with water on Cu–I–TiO_2 catalyst.

sources. The existence of CH_3Cl was identified through a GC/MS measurement and calibrated by a standard (2000 μg/ml CH_3Cl in methanol, Restek). The measured amounts of photoreduction products under all of the experimental conditions are summarized in Table 3. The production of CH_4 was only observable under UV–vis light irradiation and was only prominent for the Cu–TiO_2 sample. The production of CH_3Cl was observable only when Cu was incorporated into the catalyst, apparently due to the use of $CuCl_2$ as the Cu precursor. The existence of Cl species was confirmed by the EDX analyses, as previously described. The yield of CH_3Cl for the Cu–I–TiO_2 samples increased with the concentration of Cu (and Cl) on the catalyst. In an additional experiment using $Cu(NO_3)_2$ as the Cu precursor for the catalyst (i.e., $1Cu^{NO3}$–10I–TiO_2), no formation of CH_3Cl was observed, while adding KCl together with $Cu(NO_3)_2$ (i.e., $1Cu^{NO3+KCl}$–10I–TiO_2) in the catalyst precursor resulted in the formation of CH_3Cl (see Table 3). These results again confirmed that the source of Cl in CH_3Cl was from the precursor solution.

This work is the first published document to report the formation of CH_3Cl as a result of CO_2 photoreduction on Cu-loaded TiO_2 when a chlorinated precursor was used. The formation of a Cl-labeled final product (CH_3Cl) may provide unique insights into the reaction mechanism of CO_2 reduction that has not previously been articulated in the literature. The path to CH_3Cl formation is likely through the reaction of a methyl radical ($CH_3^{\bullet}$) and a chlorine radical ($Cl^{\bullet}$). The generation of $Cl^{\bullet}$ is a result of the oxidation of chloride ions with photo-induced holes [41–43]. $CH_3^{\bullet}$ was reported to be one of the reaction intermediates for CO_2 photoreduction to CH_4 on TiO_2, and was confirmed by electron paramagnetic resonance (EPR) spectroscopy [7,44,45]. The possible reaction pathways during the CO_2 reduction process in this work are listed as follows, and the reaction mechanism is illustrated in Fig. 6.

$$TiO_2 \xrightarrow{h\nu} e_{cb}^- + h_{vb}^+ \quad (1)$$

$$H_2O_{(g)} \rightarrow H_2O_{(ads)} \quad (2)$$

$$CO_{2(g)} \rightarrow CO_{2(ads)} \quad (3)$$

$$2H_2O_{(ads)} + 4h^+ \rightarrow 4H^+ + O_{2(g)} \quad (4)$$

$$H_2O_{(ads)} + e^- \rightarrow H^{\bullet} + OH^- \quad (5)$$

$$CO_{2(ads)} + 2H^+ + 2e^- \rightarrow CO_{(ads)} + H_2O_{(ads)} \quad (6)$$

$$CO_{(ads)} \rightarrow CO_{(g)} \quad (7)$$

$$CO_{(ads)} + e^- \rightarrow \{C^{\bullet}_{(ads)}\} \quad (8)$$

$$C^{\bullet}_{(ads)} + H^{\bullet} \rightarrow \{CH^{\bullet}, CH_2^{\bullet}\} \rightarrow CH_3^{\bullet} \rightarrow CH_{4(g)} \quad (9)$$

$$Cl^- + h^+ \rightarrow Cl\cdot \quad (10)$$

$$CH_3\cdot + Cl\cdot \rightarrow CH_3Cl_{(g)} \quad (11)$$

Table 3
Amounts of CO_2 photoreduction products measured at 210 min under visible and UV–vis light irradiation.

Sample	Visible light irradiation			UV/vis light irradiation		
	CO $\mu mol\,g^{-1}$	CH_3Cl $\mu mol\,g^{-1}$	CH_4 $\mu mol\,g^{-1}$	CO $\mu mol\,g^{-1}$	CH_3Cl $\mu mol\,g^{-1}$	CH_4 $\mu mol\,g^{-1}$
TiO_2	0	0	0	0.7	0	0
10I–TiO_2	5.3	0	0	3.9	0	0
1Cu–TiO_2[a]	0	0	0	1.8	0.49	0.38
0.1Cu–10I–TiO_2[a]	4.0	0.08	0	12.0	0	0
0.5Cu–10I–TiO_2[a]	2.0	0.24	0	9.4	0.12	0.04
1Cu–10I–TiO_2[a]	6.7	0.38	0	5.4	0.15	0.04
$1Cu^{NO3}$–10I–TiO_2[b]	n/m	n/m	n/m	1.5	0	0.09
$1Cu^{NO3+KCl}$–10I–TiO_2[c]	1.5	0.26	0	n/m	n/m	n/m

n/m: not measured.
[a] $CuCl_2$ was used as the Cu precursor.
[b] $Cu(NO_3)_2$ was used as the Cu precursor.
[c] $Cu(NO_3)_2$ and KCl were used as the precursor with Cu:Cl = 1:2.

$$CH_{4(g)} + 2Cl\cdot \rightarrow CH_3Cl_{(g)} + HCl_{(g)} \quad (12)$$

Reactions (1)–(8) suggest that CO_2 is first reduced to CO through a two-electron and two-proton reaction, which can be further reduced to surface adsorbed C species. These adsorbed C species are intermediates for the generation of CH_4 and CH_3Cl present in the final products (reactions (9)–(11)). The produced amounts of CH_4 and CH_3Cl are far less than that of CO since CO is possibly the precursor. The produced amount of CH_3Cl is generally higher than that of CH_4 (Table 3). This result may be because of two reasons: (1) $Cl^{\bullet}$ reacts with $CH_3^{\bullet}$ at a higher rate than $H^{\bullet}$ does and/or the abundance of $Cl^{\bullet}$ is larger than $H^{\bullet}$, and (2) CH_4 reacts with $Cl^{\bullet}$ to yield CH_3Cl as shown in reaction (12). Nevertheless, the formation mechanism of CH_3Cl should be analogous to that of CH_4. The detection of CH_3Cl in this work verifies the EPR results in the literature [7,44,45] that indicates that $CH_3^{\bullet}$ is an intermediate species in the CO_2 photoreduction process. An additional important finding in our experiments is that the color of the catalyst turned darker during the process of CO_2 photoreduction with H_2O, and it would gradually restore to (or close to) its original color if the used catalyst was exposed to air at room temperature. The darkening in catalyst color may be an indication of the formation of intermediate C species adsorbed onto the surface. Since these species are unstable, they are difficult to measure under the experimental settings that were used. This intriguing phenomenon and the identification of reaction intermediates will be investigated in full detail in our future research by using in situ Fourier transform infrared (FTIR) spectroscopy.

To further investigate the effects of Cl species on CO_2 photoreduction, the activities of three catalysts were compared: 1Cu–10I–TiO_2 ($CuCl_2$ as the precursor), $1Cu^{NO3}$–10I–TiO_2 ($Cu(NO_3)_2$ as the precursor), and $1Cu^{NO3+KCl}$–10I–TiO_2 ($Cu(NO_3)_2$ + KCl as the precursor), and the results are as listed in Table 3. The $1Cu^{NO3}$–10I–TiO_2 catalyst had a CO production ($1.5\,\mu mol\,g^{-1}$) that was less than one third of the CO production that was observed using1Cu–10I–TiO_2 ($5.4\,\mu mol\,g^{-1}$) under UV–vis irradiation, although the yield of CH_4 was comparable. The $1Cu^{NO3+KCl}$–10I–TiO_2 catalyst also had a much lower CO production ($1.5\,\mu mol\,g^{-1}$) than 1Cu–10I–TiO_2 ($6.7\,\mu mol\,g^{-1}$) under visible light irradiation, although the produced amounts of CH_3Cl were close to each other. These results indicate that $CuCl_2$ as the Cu precursor is more effective than $Cu(NO_3)_2$. A similar finding was reported by Tseng et al. [40] that the choice of a $CuCl_2$ precursor increased the Cu dispersion and thus resulted in a higher CO_2 photoreduction rate as compared to that obtained with a copper acetate precursor. In addition to the enhanced Cu dispersion due to $CuCl_2$, the surface Cl ions act as hole-scavengers (reaction (10)) and thus help to separate the electron–hole pairs and enable more electrons to react with CO_2. The result that a mixture of $Cu(NO_3)_2$ and KCl as the Cu precursor was less effective in producing valuable products as compared to $CuCl_2$ suggests that the additional ions (NO_3^-, K+) may have a negative effect on Cu dispersion. On the other hand, using $CuCl_2$ as the precursor led to unwanted products (e.g., CH_3Cl) even though its CO production rate was about three times higher than that using $Cu(NO_3)_2$ as the precursor. Therefore, more attention should be paid by the research community to the choice of catalyst modifier precursors when undertaking CO_2 photoreduction studies.

4. Conclusion

In this work, Cu and I co-modified TiO_2 catalysts (Cu–I–TiO_2) were synthesized with iodine doped into the TiO_2 lattice and Cu deposited on the TiO_2 surface. The material properties and catalytic activities for CO_2 photoreduction with water were compared using pure TiO_2, single-ion modified TiO_2 (Cu–TiO_2 and I–TiO_2), and co-modified catalysts (Cu–I–TiO_2). Iodine doping was responsible for visible light activity of the catalyst while Cu species, mainly Cu(I), facilitated charge transfer and enhanced CO_2 reduction. However, the catalytic activity and the optimum catalyst composition under visible or UV–visible light irradiation were different. Under UV–vis irradiation, the activity of the Cu–I–TiO_2 sample was higher than that of Cu–TiO_2 or I–TiO_2, whereas, under visible light, Cu–I–TiO_2 was not always superior to I–TiO_2. To achieve an optimum activity, a lower modifier concentration is needed under UV–vis light than under visible light, possibly because a high modifier concentration may lead to the formation of recombination centers. This work identified the generation of CH_3Cl from CO_2 reduction. The Cl species was derived from $CuCl_2$, a frequently used Cu precursor. The formation of CH_3Cl suggests that surface adsorbed carbon species and methyl radicals may be reaction intermediates, which warrants follow-up investigation using in situ IR spectroscopy. While using $CuCl_2$ as the Cu precursor resulted in a much higher CO_2 photoreduction rate than using $Cu(NO_3)_2$, the undesirable CH_3Cl in the reaction products may be a concern.

Acknowledgements

This work was supported by the University of Wisconsin-Milwaukee Research Foundation Bradley Catalyst Grant (133-PRJ38QV) and the National Science Foundation (Award# 1067233 and Award # 1067340). The authors also gratefully acknowledge access to the shared facilities at the LeRoy Eyring Center for Solid State Science at Arizona State University for some of the characterization work that is reported.

References

[1] C.S. Song, Catalysis Today 115 (2006) 2–32.
[2] T. Inoue, A. Fujishima, S. Konishi, K. Honda, Nature 277 (1979) 637–638.
[3] Y. Li, W.-N. Wang, Z. Zhan, M.-H. Woo, C.-Y. Wu, P. Biswas, Applied Catalysis B: Environmental 100 (2010) 386–392.
[4] Q. Zhang, Y. Li, E.A. Ackerman, M. Gajdardziska-Josifovska, H. Li, Applied Catalysis A: General 400 (2011) 195–202.
[5] K. Kočí, K. Matějů, L. Obalová, S. Krejčíková, Z. Lacný, D. Plachá, L. Čapek, A. Hospodková, O. Šolcová, Applied Catalysis B: Environmental 96 (2010) 239–244.
[6] I.H. Tseng, W.C. Chang, J.C.S. Wu, Applied Catalysis B: Environmental 37 (2002) 37–48.
[7] M. Anpo, H. Yamashita, Y. Ichihashi, S. Ehara, Journal of Electroanalytical Chemistry 396 (1995) 21–26.
[8] K. Koci, L. Obalova, Z. Lacny, Chemical Papers 62 (2008) 1–9.
[9] V.P. Indrakanti, J.D. Kubicki, H.H. Schobert, Energy & Environmental Science 2 (2009) 745–758.
[10] T.J. Kemp, R.A. McIntyre, Polymer Degradation and Stability 91 (2006) 3010–3019.
[11] L.C.-K. Liau, C.-C. Lin, Applied Surface Science 253 (2007) 8798–8801.
[12] S. Sakthivel, M.V. Shankar, M. Palanichamy, B. Arabindoo, D.W. Bahnemann, V. Murugesan, Water Research 38 (2004) 3001–3008.
[13] A.L. Linsebigler, G.Q. Lu, J.T. Yates, Chemical Reviews 95 (1995) 735–758.
[14] Y.H. Xu, D.H. Liang, M.L. Liu, D.Z. Liu, Materials Research Bulletin 43 (2008) 3474–3482.
[15] G.H. Li, N.M. Dimitrijevic, L. Chen, T. Rajh, K.A. Gray, Journal of Physical Chemistry C 112 (2008) 19040–19044.
[16] J.C.S. Wu, Catalysis Surveys from Asia 13 (2009) 30–40.
[17] J. Choi, H. Park, M.R. Hoffmann, Journal of Physical Chemistry C 114 (2010) 783–792.
[18] B. Xin, P. Wang, D. Ding, J. Liu, Z. Ren, H. Fu, Applied Surface Science 254 (2008) 2569–2574.
[19] M. Anpo, Bulletin of the Chemical Society of Japan 77 (2004) 1427–1442.
[20] Y. Li, W. Wang, X. Qiu, L. Song, H.M. Meyer Iii, M.P. Paranthaman, G. Eres, Z. Zhang, B. Gu, Applied Catalysis B: Environmental 110 (2011) 148–153.
[21] M. Ni, M.K.H. Leung, D.Y.C. Leung, K. Sumathy, Renewable and Sustainable Energy Reviews 11 (2007) 401–425.
[22] R. Asahi, T. Morikawa, T. Ohwaki, K. Aoki, Y. Taga, Science 293 (2001) 269–271.
[23] T. Umebayashi, T. Yamaki, H. Itoh, K. Asai, Applied Physics Letters 81 (2002) 454–456.
[24] S.Z. Chen, P.Y. Zhang, D.M. Zhuang, W.P. Zhu, Catalysis Communications 5 (2004) 677–680.
[25] R. Long, Y. Dai, B. Huang, Computational Materials Science 45 (2009) 223–228.
[26] W. Su, Y. Zhang, Z. Li, L. Wu, X. Wang, J. Li, X. Fu, Langmuir 24 (2008) 3422–3428.
[27] S. Tojo, T. Tachikawa, M. Fujitsuka, T. Majima, Journal of Physical Chemistry C 112 (2008) 14948–14954.
[28] Z.Q. He, X. Xu, S. Song, L. Xie, J.J. Tu, J.M. Chen, B. Yan, Journal of Physical Chemistry C 112 (2008) 16431–16437.
[29] G. Liu, C. Sun, X. Yan, L. Cheng, Z. Chen, X. Wang, L. Wang, S.C. Smith, G.Q. Lu, H.-M. Cheng, Journal of Materials Chemistry 19 (2009) 2822–2829.
[30] K. Song, J. Zhou, J. Bao, Y. Feng, Journal of the American Ceramic Society 91 (2008) 1369–1371.
[31] M. Hamadanian, A. Reisi-Vanani, A. Majedi, Applied Surface Science 256 (2010) 1837–1844.
[32] Y. Su, Y. Xiao, Y. Li, Y. Du, Y. Zhang, Materials Chemistry and Physics 126 (2011) 761–768.
[33] S. Song, F. Hong, Z. He, H. Wang, X. Xu, J. Chen, Applied Surface Science 257 (2011) 10101–10108.
[34] O.K. Varghese, M. Paulose, T.J. LaTempa, C.A. Grimes, Nano Letters 9 (2009) 731–737.
[35] K. Lalitha, G. Sadanandam, V.D. Kumari, M. Subrahmanyam, B. Sreedhar, N.Y. Hebalkar, Journal of Physical Chemistry C 114 (2010) 22181–22189.
[36] T.V. Nguyen, J.C.S. Wu, Solar Energy Materials and Solar Cells 92 (2008) 864–872.
[37] H.Z. Zhang, J.F. Banfield, Journal of Physical Chemistry B 104 (2000) 3481–3487.
[38] L. Zhou, J. Deng, Y. Zhao, W. Liu, L. An, F. Chen, Materials Chemistry and Physics 117 (2009) 522–527.
[39] Slamet, H.W. Nasution, E. Purnama, S. Kosela, J. Gunlazuardi, Catalysis Communications 6 (2005) 313–319.
[40] I.H. Tseng, J.C.S. Wu, H.Y. Chou, Journal of Catalysis 221 (2004) 432–440.
[41] J. Moser, M. Gratzel, Helvetica Chimica Acta 65 (1982) 1436–1444.
[42] P. Calza, E. Pelizzetti, Pure and Applied Chemistry 73 (2001) 1839–1848.
[43] B. Neppolian, H.C. Choi, S. Sakthivel, B. Arabindoo, V. Murugesan, Chemosphere 46 (2002) 1173–1181.
[44] N.M. Dimitrijevic, B.K. Vijayan, O.G. Poluektov, T. Rajh, K.A. Gray, H.Y. He, P. Zapol, Journal of the American Chemical Society 133 (2011) 3964–3971.
[45] H. Yamashita, H. Nishiguchi, N. Kamada, M. Anpo, Y. Teraoka, H. Hatano, S. Ehara, K. Kikui, L. Palmisano, A. Sclafani, M. Schiavello, M.A. Fox, Research on Chemical Intermediates 20 (1994) 815–823.